Design and experimental verification of a fuel cell/supercapacitor passive configuration for a light vehicle

Journal of Energy Storage 33 (2021) 102110

Contents lists available at ScienceDirect

Journal of Energy Storage

journal homepage: www.elsevier.com/locate/est

Design and experimental verification of a fuel cell/supercapacitor passive configuration for a light vehicle

Qian Xun *, Stefan Lundberg, Yujing Liu

Department of Electrical Engineering, Chalmers University of Technology, 41279, Gothenburg, Sweden

ARTICLE INFO

Keywords:
Fuel cell
Supercapacitor
Passive configuration
Power distribution
Drive cycle

ABSTRACT

The fuel cell/supercapacitor passive configuration without using any DC/DC converters is promising in automotive applications as it can downsize the fuel cell stack, maintain the peak power capability, improve the system efficiency, and remove the need of additional control. This paper presents the design and characterization of a fuel cell/supercapacitor passive hybrid system for a 60 V light vehicle. A detailed design procedure for the passive hybrid test platform is presented with each component modelled and experimentally verified. The voltage error of the fuel cell and the supercapacitor model in the steady state is within 2% and 3%, respectively. Experimental results also validate the function of the passive configuration under conditions of a step load and a drive cycle. The simulation model of the passive hybrid system matches the measurements when a step load current is applied. The supercapacitor provides the transient current due to its smaller resistance while the fuel cell handles the steady state current, which makes it possible to downsize the fuel cell stack. For the drive cycle examined in this paper, the fuel cell stack can be downsized to one third of the load peak power.

1. Introduction

The rapid development of the automotive industry has led to a larger number of vehicles worldwide. Internal combustion engine (ICE) vehicles have been very popular and widely used during the past decades. However, there are a few environmental issues associated with the growing usage of ICE vehicles, which include oil depletion and air pollution from greenhouse gas (GHG) emissions, fine particles, and smog. The world crude oil reserves are projected to run out in the next forty years [1], which makes the development of alternative and sustainable energy resources essential.

Transportation electrification is one of the most promising approaches to reduce the impacts of air pollution and fossil fuel consumption. Among others, two types of all-electric vehicles (EVs) are based on battery and fuel cell (FC) technologies [2]. Fuel cell electric vehicles (FCEVs) are efficient, environmentally friendly, and zero-emissions as they only emit water and heat [3–5]. In such vehicles, the FC can be used along with a battery or a supercapacitor (SC). This is because the relatively slow dynamic response and the inability to recover regenerative braking energy of the FC make it challenging to meet the varying power demands of the vehicle. Therefore, it is necessary to use a battery, an SC or both together with the FC.

There are three hybridization configurations: fully active, semi-active, and passive depending on the number of DC/DC converters used and the way in which the components are connected to the DC bus [6]. The fully active hybrid system is fully controllable since DC/DC converters are associated with each power source. The semi-active hybrid system with a reduced number of DC/DC converters, can only control the DC-link voltage and the power distribution indirectly. In the passive configuration without any DC/DC converters, power distribution is inherently decided by the characteristics of each device. In the early years of commercial FC electric cars (e.g., Honda FCX [7,8]), FC and SC are hybridized. Later, FC and battery are used in Honda FCX Clarity, Honda Clarity Fuel Cell [9], Toyota FCHV-adv, Toyota Mirai [10,11], and Hyundai NEXO [12] where semi-active or fully active hybrid topologies are employed. In such car models, one DC/DC converter is used for the battery, and the FC is directly connected or connected through one DC/DC converter to the DC bus. The concept of the FC/SC passive hybrid configuration is firstly employed in Honda FCX even though one DC/DC converter is adopted between the FC and the SC. The DC/DC converter is used to pre-charge or electrically disconnect the SC when there is a voltage difference at start-up and regeneration. During the propulsion mode, the converter makes the FC and SC passively connected.

In fully active and semi-active hybrid systems, it is possible to

* Corresponding author.
E-mail addresses: qian.xun@chalmers.se (Q. Xun), stefan.lundberg@chalmers.se (S. Lundberg), yujing.liu@chalmers.se (Y. Liu).

https://doi.org/10.1016/j.est.2020.102110
Received 17 July 2020; Received in revised form 9 November 2020; Accepted 12 November 2020
Available online 7 December 2020

Nomenclature

EV	Electric vehicle
FC	Fuel cell
FCEV	Fuel cell electric vehicle
ICE	Internal combustion engine
GHG	Greenhouse gas
MPC	Model predictive control
OCV	Open circuit voltage
PEM	Proton exchange membrane
SC	Supercapacitor
SoC	State-of-charge
SPS	Sim Power Systems

actively control the DC-link voltage and power distribution directly or indirectly. Therefore, advanced power control and energy management strategies are required in such topologies. For example, [13] compares two FC/battery semi-active hybrid topologies and the experimental results show that the topology with a direct battery connection has better fuel economy. This topology is also examined in [14,15] and model predictive control (MPC)-based strategies are used to minimize the hydrogen consumption, FC degradation, and battery state-of-charge (SoC) fluctuations. In [16], convex programming is used to optimize the power-split strategy between the FC and the battery pack. Similarly, FC/SC semi-active hybrid topologies are studied along with various power control methods in [17,18]. A fully active FC/battery hybrid topology is investigated in [19]: the total running cost is optimized based on a MPC framework and the impacts of driving and pricing are also explored. Also, the fully active FC/SC configuration is studied in [20,21] for an electric tram. Moreover, FC/battery/SC active hybrid topologies with two or three DC/DC converters are proposed in [22–25] and different control strategies are employed to improve the overall performance. Detailed energy management strategies along with future research trends are summarized in [26]. Clearly, active and semi-active hybrid configurations require a robust control strategy and additional DC/DC converters to improve the control performance. However, using DC/DC converters results in additional energy losses and increases the system weight, volume, and cost [27–29].

Since no DC/DC converters are used, the passive configuration can mitigate the issues above. Moreover, the passive configuration provides a natural power split depending on the internal resistance of each device. In Fig. 1, an example of a passive hybrid powertrain is shown where no DC/DC converters are used. To ensure that the FC and the battery/SC are properly operating (e.g., their operating voltage ranges are similar and their SoC are suitable), the hybrid configuration needs to be carefully designed [30]. Since the power distribution of each device cannot be actively controlled in the passive configuration, a power control method in an FC/battery passive hybrid system is developed in [31] and the power distribution can be indirectly controlled by the FC working pressure. However, this method makes the FC operating pressure lower than nominal. In [32], the passive configuration of an FC and a Li-ion battery is studied, and the open-circuit voltage (OCV) of the FC is 10 V higher than that of the battery. To avoid overcharging the battery, a MOSFET is used between the FC and the battery to determine the operating mode: FC only or FC/battery hybrid. Usually, the passive hybrid system combining an FC and a battery is promising in unmanned vehicles operating around 24 VDC and with a peak power of up to 1.5 kW. In these cases, it is possible to find FCs and batteries that can operate within a similar voltage range if the battery with a suitable capacity is charged with the maximum current provided by the FC [31–34].

Due to its wide operating voltage range, SC is well-suited to directly hybridize with FC. Moreover, this combination is suitable for frequent start/stop occasions since SC can provide high transient power with a long cycle life [35]. Therefore, the FC/SC passive configuration can be used to downsize the FC stack, reduce the fuel overconsumption, avoid flooding inside the FC, and improve the FC lifetime [27,36,37]. In [38–40], the FC/SC passive configuration is analyzed, sized, and modelled at the cell level. A global system sizing approach for FC and SC is proposed in [41] based on a pre-defined automotive power profile. An FC/SC passive configuration with a 9.5 kW FC stack is developed in [42] and the feasibility under a downscaled drive cycle power profile is experimentally performed.

To obtain a functional passive power split, the sizing of FC and SC in such topology is important. The basic criteria include the DC-link voltage and the energy storage capacity. Moreover, the FC operating current dynamics is proposed in [43] as the third design criterion. This work also develops a lab-scaled FC/SC prototype based on the power profile measured from a Nemo EV. A detailed analysis of an EV with FC/SC passive configuration is performed in [44]; the model of each component is studied, and the power distribution and dynamic characteristics are evaluated at the system level. Due to the unique characteristics of FC and SC, the DC-link voltage is passively determined by the power distribution, which is highly dependent on the driving cycle. Therefore, the energy efficiency of a powertrain system with passive hybridization of FC and SC is analyzed and evaluated based on different drive cycles, and hydrogen consumption and DC-link voltage variation are also demonstrated [45].

Existing studies on the FC/SC passive configuration are mainly focused on component sizing, initial voltage connection, component modelling and powertrain system modelling. However, previous experimental works have been limited to investigating the validation of power consumption on the hybrid configuration while the effects of regenerative power have not been well addressed [42,43]. This paper fills this gap and considers an FC/SC passive configuration for a 60 V light vehicle. The contribution of this work is to present a detailed design procedure for the test platform with each component modelled and experimentally characterized. The FC/SC passive configuration is experimentally validated using a step load current and the Artemis Urban drive cycle. Moreover, the operation of this passive configuration is verified with the regenerative power introduced into the step load

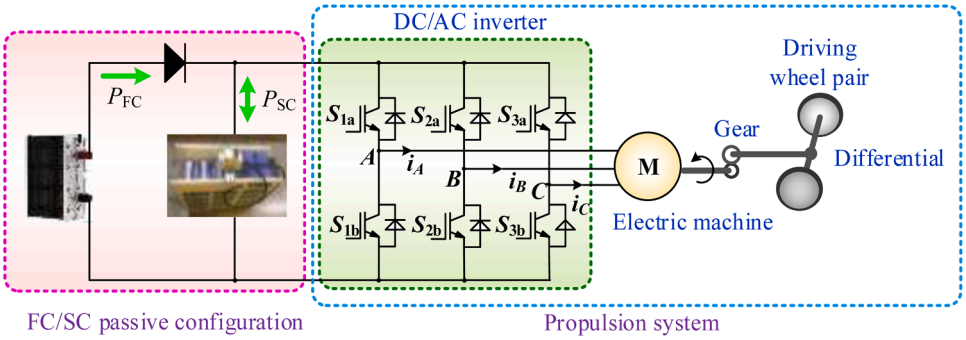

Fig. 1. Passive hybrid fuel cell/supercapacitor powertrain.

Table 1
Main specifications of Renault Twizy Urban 80.

Parameter	Value	Parameter	Value
Gross weight (kg)	690	Top speed (km/h)	80
Peak power (kW@2100 rpm)	13	Size (m^3)	2.338 × 1.397 × 1.454
Aerod. drag coeff. C_d	0.64	Ground clearance (m)	0.12
Rolling resist. coeff. C_r	0.012	Front area A_f (m^2)	~1.86

current test scenario.

The remainder of the paper is organized as follows. Section 2 is dedicated to the system configuration and the development of the test platform for each component. Section 3 presents the models of the FC, SC, and the passive hybrid system as well as the analysis of the system stability. Section 4 shows the experimental results using the step load current and the drive cycle for the hybrid system. Finally, conclusions are drawn in Section 5. Challenges and future trends of FCEVs are presented in Section 6.

2. Development of test platform

2.1. System configuration

For the analysis in this paper, Renault Twizy Urban 80 is selected as the benchmark vehicle and its main specifications [46,47] are listed in Table 1. Twizy is an all-EV and its battery pack is replaced with the FC/SC passive configuration in the case study. The passive hybrid powertrain, also considered in our previous work [2,44,45], consists of an FC stack, a diode, an SC bank, and a propulsion system including a DC/AC inverter, an electric machine, a transmission, and wheels, as shown in Fig. 1. The objective of this paper is to evaluate the FC/SC passive configuration from both experiments and simulations. The propulsion system is considered as the load, which is simulated as a controlled current source for simplicity in this study.

According to vehicle dynamics, the instantaneous wheel power P_{wheel} [48] can be derived as

$$P_{wheel} = F_{wheel} v = \left(\frac{1}{2}\rho_a C_d A_f v^2 + C_r mg\cos\alpha + m\frac{dv}{dt} + mg\sin\alpha\right)v, \quad (1)$$

where ρ_a is the air density with the value of 1.225 kg/m^3 when the dry air is under 15 °C and standard atmosphere pressure, C_d is the aerodynamic drag coefficient, A_f is the front area, v is the vehicle speed, C_r is the rolling resistance coefficient[1], m is the vehicle mass, g is the gravitational constant with the value of 9.81 m/s^2, and α is the slope with zero on a flat road. Once the vehicle speed is known, the wheel power can be calculated. Together with the energy conversion efficiency, η, the wheel power determines the power demand of the FC/SC passive hybrid system. In this study, η is assumed to be 0.9 in the propulsion mode and 0.6 in the regenerative braking mode, respectively.

2.2. Design criteria

2.2.1. Specifications of fuel cell

Proton exchange membrane (PEM) FCs are the most attractive candidate for automotive applications. This is mainly because the low operating temperature of this technology enables the fast starting from the idle state to the full power operation mode. The Horizon H-3000 FC stack is used in this study and its specifications are shown in Table 2.

2.2.2. Specifications of supercapacitor

The Maxwell BCAP3000 SCs are selected. Each of them has a rated voltage of 2.7 V and a rated capacitance of 3000 F. The detailed cell parameters can be found in [52]. To make sure that the SC bank is not overcharged, the voltage applied over it should always be within the rated range and the following equations should be met

$$\begin{cases} V_{SCB} > V_{fc} \\ V_{SCB} = V_{SC} \cdot N_{SC} \end{cases}, \quad (2)$$

where V_{SCB} is the OCV of the SC bank, V_{fc} is the maximum voltage of the FC stack, V_{SC} is the OCV of the SC cell, and N_{SC} is the number of SC cells. Then, the minimum number of cells needed is 25.33 according to (2). Therefore, 26 cells are connected in series, giving the SC bank a rated voltage of 70.2 V. The total capacitance of the SC bank with series-connected SC cells can be calculated as

$$C_{SCB} = \frac{1}{\sum_{i=1}^{N_{SC}} \frac{1}{C_i}}, \quad (3)$$

where C_i is the capacitance of each individual SC cell. The total energy of the SC bank is

$$E_{SCB} = \frac{1}{2} \times C_{SCB}\left(V_{SCB\_max}{}^2 - V_{SCB\_min}{}^2\right), \quad (4)$$

where V_{SCB_max} and V_{SCB_min} are the maximum and minimum operating voltage of the SC bank, respectively. The SC bank is connected in parallel with the FC stack, which means that it can only operate within the FC voltage range from 36 V to 68.4 V. Therefore, the total energy of the SC bank is 195 kJ with the total capacitance of around 115 F. The total internal resistance of the SC bank is 7.54 mΩ.

2.3. Fuel cell test platform

The FC test platform is shown in Fig. 2. The H-3000 air-breathing FC stack from Horizon Technology is tested, a 10 L HYDROGEN 6.0 hydrogen tank with an initial pressure of 200 bar from Aga Gas AB is used to provide hydrogen to the FC stack, and a two-stage pressure regulator is connected to adjust the hydrogen pressure from the tank. The first stage is to generate a pressure between 0~40 bar, and the second stage is to tune the pressure to around 0.5 bar. During the FC operation, the unreacted hydrogen needs to be purged out from the purge valve, and the output of the purge valve is connected to the outside to avoid the accumulation of hydrogen gas in the lab. The electronic load, EA-9000HP, is connected to provide the dynamic current to the FC stack. The FC controller is used to control the supply valve, purge valve, and air fans as well as to detect the voltage, current, and temperature of the FC stack. The experimental data is collected by

Table 2
Technical specifications of H-3000 [51].

Parameter	Value
Type of fuel cell	PEM
Number of cells	72
Voltage range	68.4~36 V
Rated power	3 kW
Rated performance	70 A @ 43.2 V
Max-current (shutdown)	90 A @ 36 V
Hydrogen pressure	0.45 ~ 0.55 bar
Rated H_2 consumption	39 L/min @ SLPM [a]
Ambient temperature	22 °C
Max-stack temperature	65 °C
Cooling	Air (integrated cooling fan)

[a] SLPM means standard liter per minute, which is a unit of the volumetric flow rate of a gas at standard conditions for temperature and pressure.

[1] Empirical studies show that C_r depends on the tire material, design, and working conditions [49]. At low speed levels, C_r increases only slightly with the speed while it is proportional to almost the square of the speed at relatively high speed levels [50]. C_r is often assumed to be constant to study the vehicle performance and fuel economy.

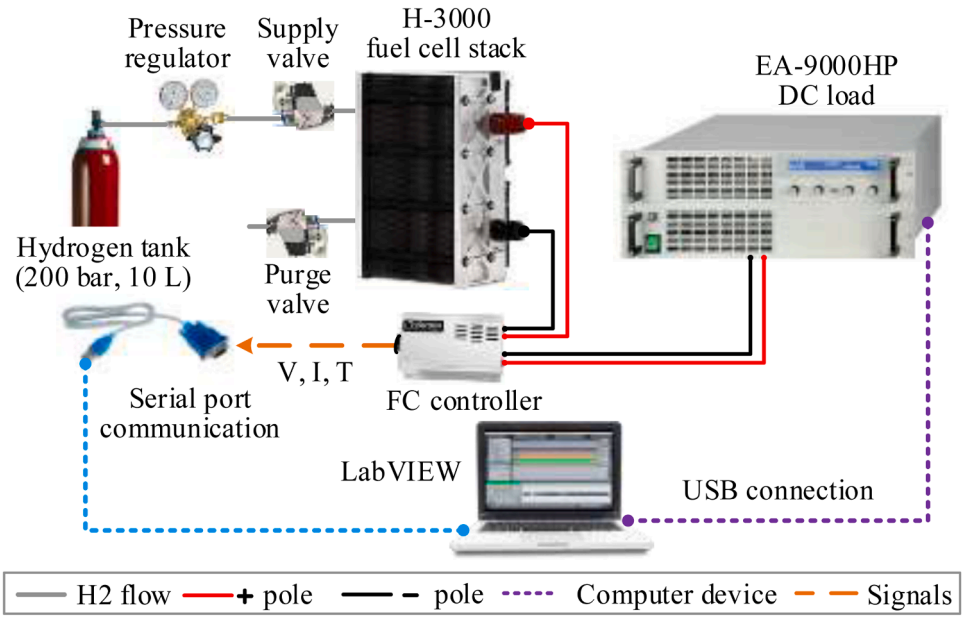

Fig. 2. Test platform for fuel cell stack.

LabVIEW through serial port communication.

2.4. Supercapacitor test platform

The SC bank is tested using the platform shown in Fig. 3. Two DC power supplies, SM30-200, are connected in series to generate a maximum voltage of 60 V. The EA-9000HP is connected in parallel to discharge the SC bank. The oscilloscope is used to collect the experimental data. The SC bank is charged and discharged by a constant current of 50 A. The SC bank is charged to the maximum voltage of about 60 V and discharged to 6 V.

2.5. Implementation of passive hybrid configuration

Separate measurements are firstly conducted on the FC stack and the SC bank as shown in Figs. 2 and 3. Then, the FC system, the SC bank, the power supply, and the electronic load are connected to form a passive hybrid system. The schematic of the experimental setup is shown in Fig. 4. The diode, MUR2X100A02, is used to prevent the energy exchange from the SC bank to the FC stack and the power supply. The DC breakers are used to connect or disconnect the separate devices. Since the maximum current of the electronic load is 50 A, the C65N-DC DC breaker with a rated current of 63 A is selected.

To prevent the inrush current when the system starts up, the SC bank is pre-charged at the beginning. The process to run the system is listed as below:

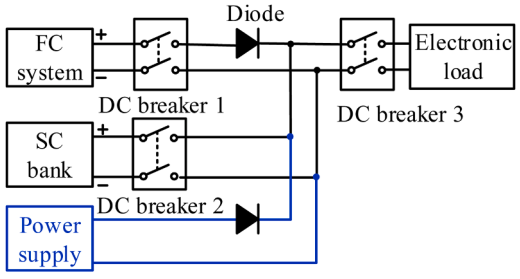

Fig. 4. Schematic of the experimental setup for fuel cell/supercapacitor passive hybrid configuration.

Step 1. Connect the cables and make sure that all the components are correctly connected. Also, make sure that the FC system, the SC bank, and the electronic load are electrically disconnected;

Step 2. Turn on the power supply and pre-charge the SC bank to at least 50 V. In case of high currents at the system start-up, the SC bank is pre-charged to 60 V in this study;

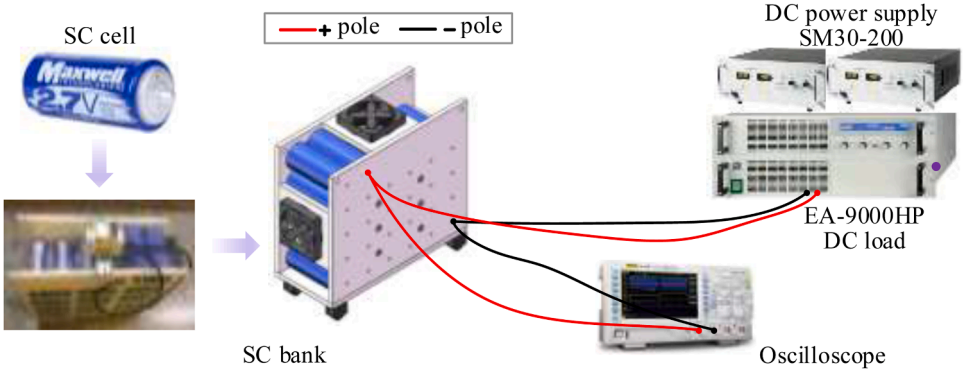

Fig. 3. Test platform for supercapacitor bank.

Step 3. Turn off the power supply and turn on the FC system;

Step 4. Close breaker 1 and breaker 2 to balance the voltages of the FC stack and the SC bank. They should have the same equilibrate voltage of approximately 68 V;

Step 5. Close breaker 3 to electrically connect the FC system, the SC bank, and the electronic load. Turn on the electronic load, apply the dynamic load, and run the system;

Step 6. After all the tests have been done, reduce the load current to zero, open breaker 1, and turn off the FC system;

Step 7. Now only the SC bank is connected to the electronic load. Apply a load current to discharge the SC bank;

Step 8. When the SC bank is fully discharged, open breaker 2 and breaker 3, and turn off the electronic load.

3. System modelling and characterization

3.1. Fuel cell modelling and characterization

3.1.1. Modelling

The FC stack uses the generic FC model provided in the Sim Power Systems (SPS) toolbox of MATLAB/Simulink [53]. The model contains a controlled-voltage source connected in series with an internal resistor, as shown in Fig. 5. The output voltage [54–56] is expressed as

$$V_{fc} = E_{oc} - V_{act} - V_{ohmic}, \tag{5}$$

$$\text{with} \begin{cases} E_{oc} = K_c\left(1.229 + (T-298)\cdot\dfrac{-44.43}{2F} + \dfrac{RT}{2F}\ln(P_{H_2}P_{O_2}^{1/2})\right) \\ V_{act} = NA\ln\left(\dfrac{i_{fc}}{i_0}\right)\cdot\dfrac{1}{\tau s+1} \\ V_{ohmic} = r_{fc}\cdot i_{fc} \end{cases}, \text{ where}$$

V_{fc} is the stack output voltage, E_{oc} is the stack open-circuit voltage, V_{act} is the activation voltage loss of the stack, and V_{ohmic} is the ohmic voltage loss. As shown in Fig. 5, E_{oc}-V_{act} is modelled as the controlled voltage source E. K_c is the nominal voltage constant. T is the stack operating temperature, F is the Faraday constant, R is the ideal gas constant, P_{H2} is the partial pressure of the hydrogen, and P_{O2} is the partial pressure of the oxygen. N is the number of cells, A denotes the Tafel slope, i_{fc} is the stack output current, i_0 is the exchange current, τ is the time constant of the stack dynamic response, and r_{fc} is the internal resistance of the stack.

3.1.2. Characterization

The model parameters are obtained from the tested polarization curve of the FC stack. Fig. 6 (a) compares the measured and simulated polarization curves. The stack voltage decreases gradually with the increase of the current while the stack power increases with the current. The simulation results show a good match with the experimental data with a voltage error within 2%. When step load currents are applied to the FC stack, the simulated and measured voltage profiles are shown in Fig. 6 (b). It can be observed that when the load current changes from 40 A to 50 A, the FC voltage first drops to 40.9 V instantaneously and then increases slightly to 41.5 V. When the load current changes from 50 A to 40 A, the voltage has an overshoot and then declines slightly to 44 V. Therefore, the voltage has an instantaneous change and there is a time delay for the voltage to reach the steady-state, which suggests that the FC stack behaves as a first-order system when the step load current is applied. The time delay is closely related to the temperature and the air supply subsystem. The air supply subsystem is simulated by a first-order inertial link and the temperature is considered as a constant.

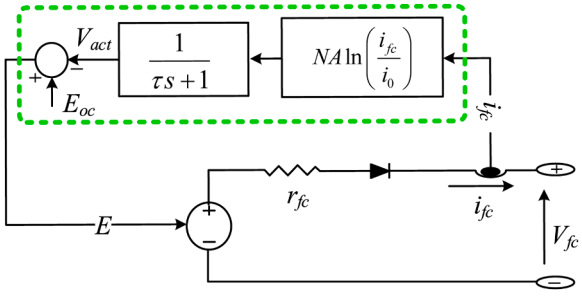

Fig. 5. Fuel cell equivalent circuit model [53].

The relationship between the voltage and the current of the FC stack can be simulated as a linear function. If the FC stack does not operate at the OCV but with a higher current, the polarization curve can be linearized to provide the linear model of the studied FC stack, which can be described as

$$V_{fc} = V_{fc0} - k_{fc}i_{fc}, \tag{6}$$

where k_{fc} is the linear coefficient shown in Fig. 7. k_{fc} is estimated to be 0.2388 Ω when the FC stack works in the ohmic region where the current is above 10 A.

3.2. Supercapacitor modelling and characterization

3.2.1. Modelling

The SC bank is represented by a generic Stern model [57,58] shown in Fig. 8, which is also available in the SPS toolbox of MATLAB/Simulink [59]. The output voltage can be obtained as follows

$$V_{SCB} = \frac{Q_{SCB}}{C_{SCB}} - r_{SCB}i_{SCB}, \tag{7}$$

where Q_{SCB} is the total electric charge, i_{SCB} is the current of the SC bank, and r_{SCB} is the internal resistance.

Considering the self-discharge phenomenon of the SC bank, the electric charge when $i_{SCB} = 0$ is modified as follows

$$Q_{SCB} = \int i_{self\_dis}dt, \tag{8}$$

$$\text{with } i_{self\_dis} = \begin{cases} \dfrac{C_{SCB}\alpha_1}{1+sr_{SCB}C_{SCB}} & \text{if } t - t_{oc} < t_3 \\ \dfrac{C_{SCB}\alpha_2}{1+sr_{SCB}C_{SCB}} & \text{if } t_3 < t - t_{oc} < t_4 \\ \dfrac{C_{SCB}\alpha_3}{1+sr_{SCB}C_{SCB}} & \text{if } t_4 < t - t_{oc} < t_5 \end{cases}, \text{ where } \alpha_1, \alpha_2, \text{ and } \alpha_3 \text{ are constants, which represent the discharge rates of the voltage during time intervals of } [t_{oc}, t_3], [t_3, t_4], \text{ and } [t_4, t_5], \text{ respectively. } t_{oc} \text{ is the initial time sample for which it can be assumed that the SC bank is connected to an open circuit, and } t_3, t_4, \text{ and } t_5 \text{ are the time samples accumulated over the time based on } t_{oc}.$$

3.2.2. Characterization

The self-discharge test is shown in Fig. 9 (a), where the SC bank is charged to 59.2 V by 50 A and then the charging current reduces to 0 A within several minutes. After this, the power supply is turned off and the SC bank voltage drops to 55.6 V as the charge redistributes. The measured and simulated dynamic characteristics are shown in Fig. 9 (b). The smallest error is obtained when C_{SCB} = 105.85 F and r_{SCB} = 0.0225 Ω. Due to the degradation of the SC cells and the resistances of the connectors and cables, the real capacitance is 10 F lower than the calculated value, and the real resistance is a bit higher than the calculated value in Section 2.2.2.

The obtained voltage error is less than 3% when the voltage is above 16 V and the voltage error is a little bit higher when the voltage

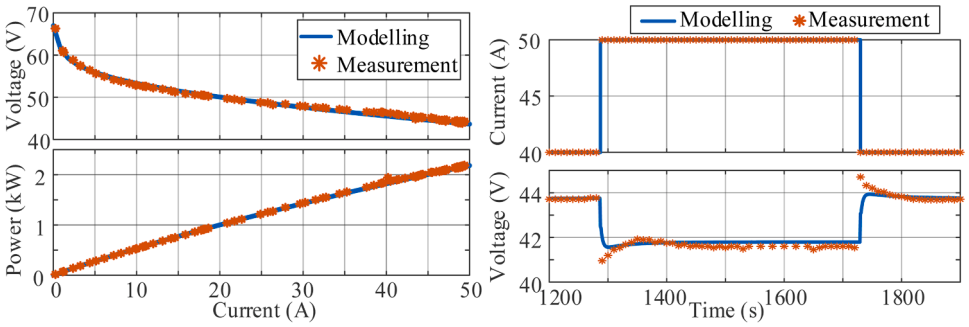

Fig. 6. Verification of fuel cell stack model: (a) Polarization curve; (b) Dynamic response.

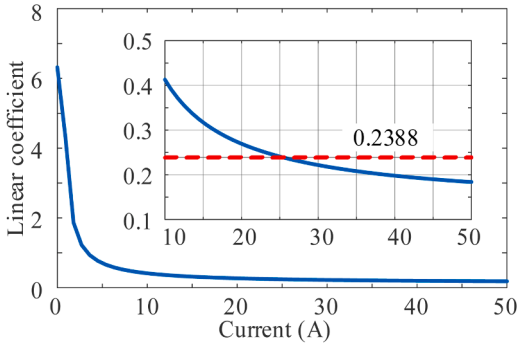

Fig. 7. Linear coefficient of the fuel cell stack.

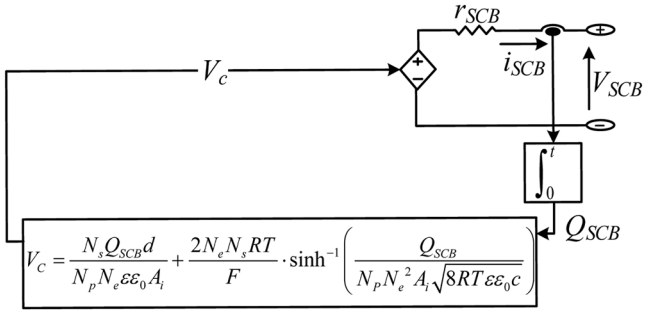

Fig. 8. Supercapacitor equivalent circuit model [59].

is below 16 V. This is because the low voltage is more difficult to model. In the meantime, the measurement error should also be considered.

3.3. System stability

In the FC/SC passive configuration, the FC stack, the SC bank, and the load are connected in parallel. Moreover, a diode is placed between the FC stack and the SC bank. Based on the component models above, the signal block diagram from the load current to the FC current is shown in Fig. 10 (a) and the signal flow graph is derived in Fig. 10 (b). Mason's gain formula depicted in Fig. 10 (c) is used to determine the transfer function:

$$G(s) = \frac{i_{fc}}{i_{load}} = \frac{1}{\Delta}\sum_k T_k \Delta_k, \tag{9}$$

where T_k is the path gain of the k^{th} forward path from the input to the output, Δ_k is the T_k path cofactor, and Δ is the determinant of the graph.

There are two forward paths (T_1 and T_2) from i_{load} to i_{fc} and three individual loops (L_1, L_2, and L_3). T_1 and T_2 touch all the individual loops and there are no non-touching loops. Therefore,

$$\begin{cases} T_1 = \dfrac{r_{SCB}}{r_D} & L_1 = -\dfrac{r_{SCB}}{r_D} & \Delta_1 = 1 \\ T_2 = \dfrac{1}{sC_{SCB}r_D} & L_2 = -\dfrac{1}{sC_{SCB}r_D} & \Delta_2 = 1 \\ & L_3 = -\dfrac{k_{fc}}{r_D} & \Delta = 1 - L_1 - L_2 - L_3 \end{cases}, \tag{10}$$

(9) can be written as

$$G(s) = \frac{1 + sC_{SCB}r_{SC}}{1 + sC_{SCB}\left(k_{fc} + r_{SCB} + r_D\right)}. \tag{11}$$

Since $r_{SCB} << k_{fc}$, the transfer function is a low-pass filter and the cut-off frequency is $1/(2\pi C_{SCB}(r_{SCB}+k_{fc}))$ by ignoring the diode resistance, which is 5.8 mHz with the model parameters determined above.

Due to the degradation of FC and SC, the coefficients of the transfer function shown in (11), which are influenced by the utilization rate,

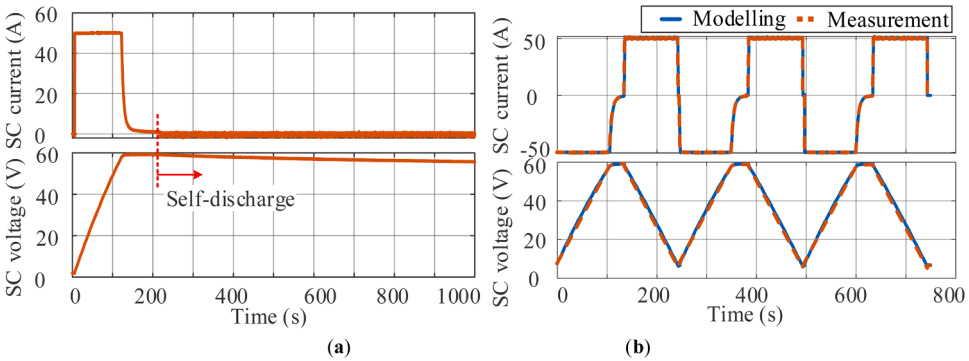

Fig. 9. Verification of the supercapacitor bank model: (a) Self-discharge test; (b) Dynamic response.

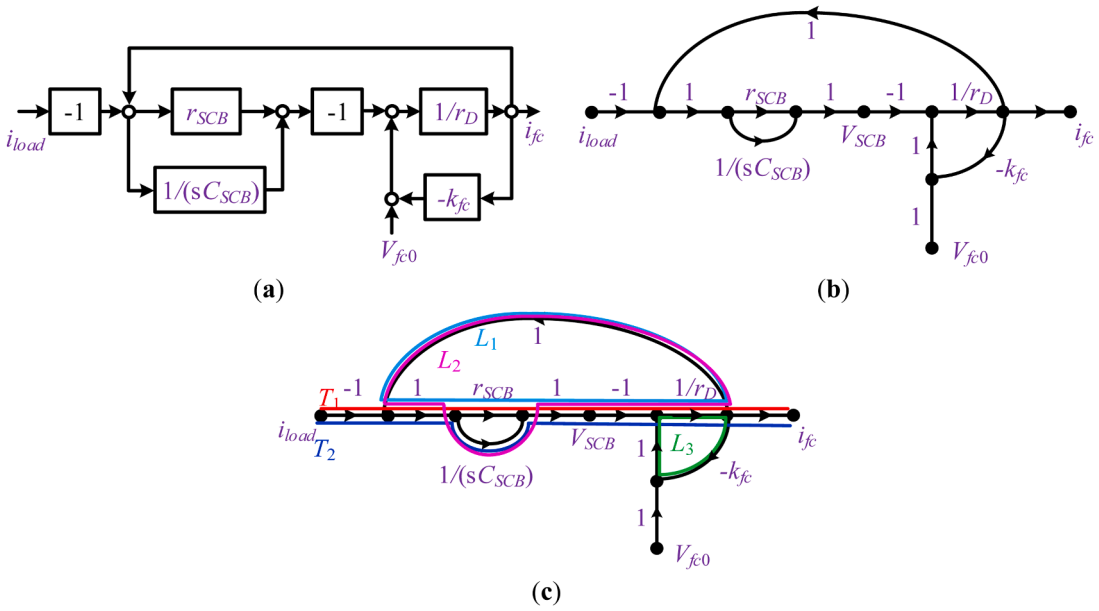

Fig. 10. Signal flow from load current to fuel cell current: (a) Signal block diagram; (b) Signal flow graph; (c) Mason's gain formula.

have a certain degree of uncertainty. This means that the precise values of C_{SCB}, r_{SCB} and k_{fc} cannot be determined readily. Empirical data shows that the SC performance degrades when its capacitance decreases and ESR increases [60]. The FC end of life is defined with respect to 10% of its voltage drop at the nominal current, which means that its internal resistance increases due to degradation [61].

Suppose the ranges of C_{SCB}, r_{SCB} and k_{fc} are given as

$$\begin{cases} C_0 - \delta_1 \le C_{SCB} \le C_0 \\ r_0 \le r_{SCB} \le r_0 + \delta_2 \\ k_0 \le k_{fc} \le k_0 + \delta_3 \end{cases}, \tag{12}$$

where $\delta_i > 0 (i = 1, 2, 3)$ and δ_i is constants for a given time interval. Therefore, by ignoring the diode resistance, the actual controlled object $(\Sigma_0, \Delta\Sigma)$ can be described as

$$G(s) = \frac{1 + s(C_0 + \Delta C)(r_0 + \Delta r)}{1 + s(C_0 + \Delta C)(r_0 + \Delta r + k_0 + \Delta k)}, \ |\Delta C| \le \delta_1, \ |\Delta r| \le \delta_2, \ |\Delta k| \le \delta_3 \tag{13}$$

The nominal system Σ_0 is described as

$$G_0(s) = \frac{1 + sC_0 r_0}{1 + sC_0(r_0 + k_0)}, \tag{14}$$

and the set of uncertainties can be described as a parameter vector set:

$$\Delta\Sigma \triangleq \{(\Delta C, \Delta r, \Delta k) || \Delta C| \le \delta_1, |\Delta r| \le \delta_2, |\Delta k| \le \delta_3\}. \tag{15}$$

Therefore, (13) can be written as

$$G(s) = G_0(s) + \Delta G(s), \tag{16}$$

with $\Delta G(s) = G(s) - G_0(s)$. According to (14), the nominal system Σ_0 has a negative pole of $-1/(C_0(r_0 + k_0))$ located in the left half of the complex plane, which means that Σ_0 is stable. Also, the uncertainty system $\Delta\Sigma$ is stable. Therefore, the actual object $(\Sigma_0, \Delta\Sigma)$ is stable and not influenced by parameter variations.

4. Evaluation of passive configuration

4.1. Step load evaluation

To evaluate the performance of the FC/SC passive hybrid configuration, the FC stack and the SC bank are connected in parallel following the procedure mentioned in the second part, and the experiment is conducted using step load currents. Note that the FC stack, the SC bank, the power supply, and the electronic load are connected in parallel and they share the same voltage theoretically. Therefore, only the load voltage is measured. The test results are shown in Fig. 11 (a). When the positive load current is applied during 20 ~ 354 s, the FC and SC together provide the current to the electronic load. The SC bank responds instantly and supplies almost all the current and power due to its smaller internal resistance. Since the SC bank supplies almost the load power, its state of charge decreases, which ultimately results in a decrease in its voltage. The system voltage is always below 60 V, which means that the FC stack does not operate at the OCV because of the long stabilization time of approximately 120 s, as shown in the figure. This can protect the FC stack against gas starvation and degradation. From the polarization curve of the FC stack, it can be observed that its current increases when its voltage decreases. In this way, the FC current increases gradually to the steady-state due to the reduced system voltage and the FC does not suffer from any current or power transients. When the negative load current is applied during 356 ~ 400 s, the SC bank is charged by this load current and the voltage of the SC bank increases. This results in the decreased FC current until a new operation equilibrium is reached. In summary, the SC bank responds to the transient current and power instantaneously while the FC stack takes over the steady-state current and power.

The current distributions obtained from the equivalent circuit model and the measurements are compared in Fig. 11 (b). In the steady state, the FC currents obtained from the equivalent circuit model have error within 4% compared to the measurements, while the errors are slightly higher during transients. This is because the resistance of the FC stack changes with the operating conditions, such as temperature, pressure, and flow rate. The resistance of the SC bank also changes with the temperature.

4.2. Drive cycle evaluation

To further evaluate the passive hybrid system, the Artemis Urban drive cycle is used to calculate the power profile for the light vehicle characterized in Table 1. The speed profile and the reference power profile considering a reduced power scale of the calculated power for the FC/SC passive configuration are shown in Fig. 12 (a). A simulation is

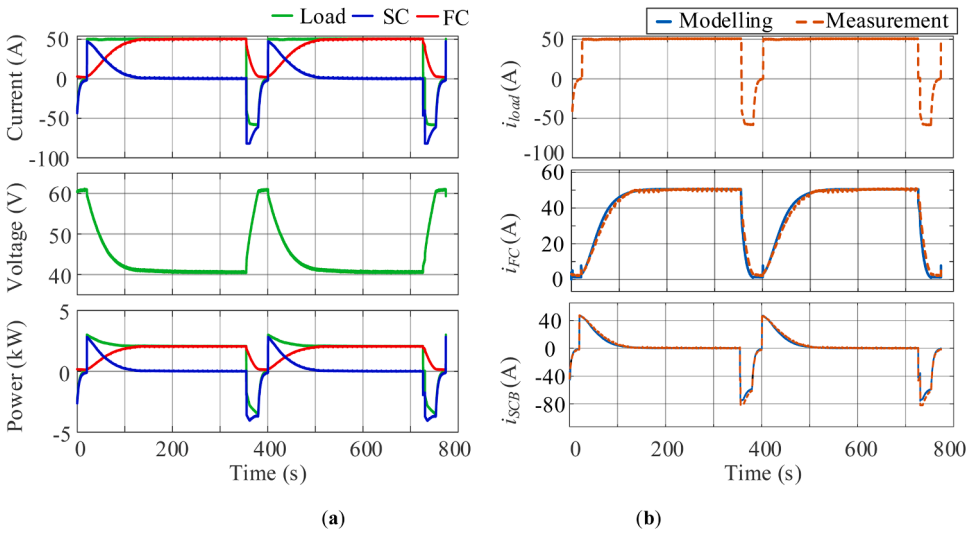

Fig. 11. Experimental results of passive hybrid system with regenerative power: (a) Measurement; (b) Current distributions.

conducted to evaluate the feasibility of the FC/SC passive configuration with the load power as the input. Before the simulation starts, the initial voltage of the SC bank is set to be 65 V to equilibrate the FC stack and the SC bank. A breakdown of the current, voltage, and power distribution for the FC stack and the SC bank can be seen in Fig. 12 (b). During the drive cycle, the FC and the SC reach a new equilibrium and the voltage is passively decided. The FC follows the load current and power. However, it does not experience the high-frequency load. This is because SC handles the high-frequency current and power.

The power histograms of the load, FC, and SC are shown in Fig. 12 (c) and "*Pct.*" represents the percentage of the specific power in the total power range. It is clear that the FC peak power is only about one third of the load peak power. This makes it possible to downsize the FC stack, i.e., for this simulation the FC stack only needs a peak power of one third of the load peak power. Also, the SC evens out the power from the FC and the FC power becomes smoother, which can reduce the fuel

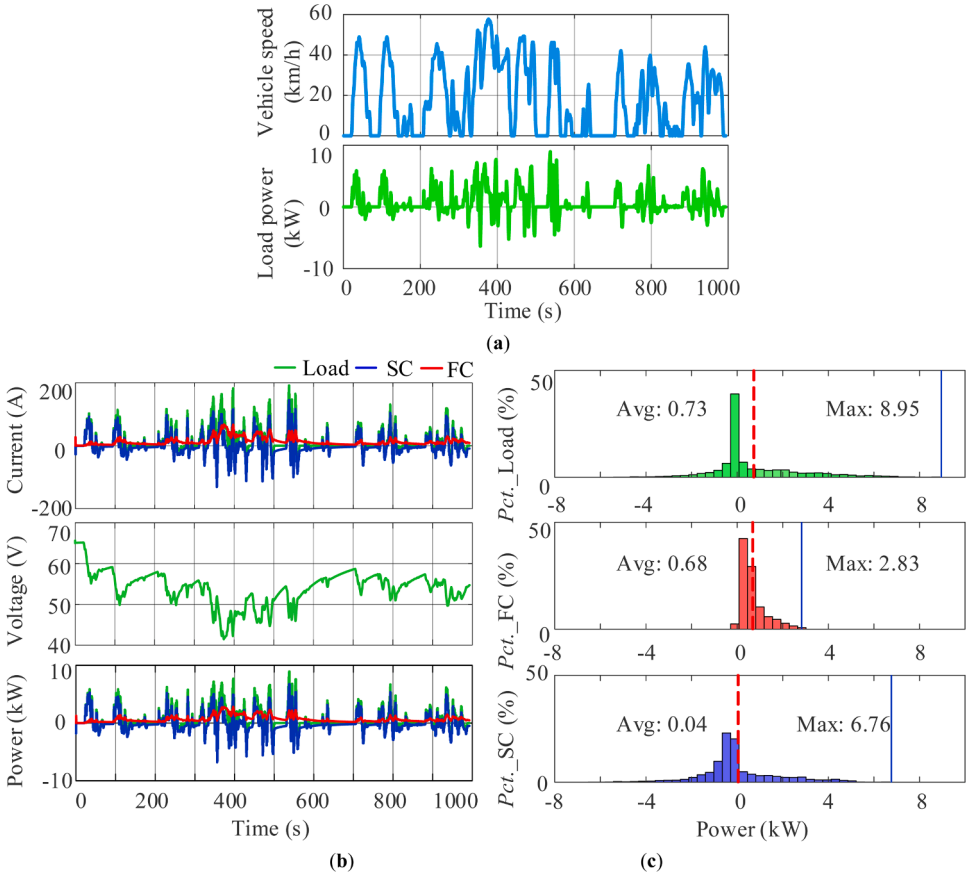

Fig. 12. Simulation results of the passive hybrid system under Artemis Urban drive cycle: (a) Vehicle speed and reference power; (b) Current, voltage and power distribution; (c) Histograms of power.

overconsumption avoid flooding inside the FC, and improve the FC lifetime [27,36,37]. The FC average power almost equals the load average power since the SC average power is only 0.04 kW. For an ideal SC, its average power should be zero. In reality, for a lossy SC, its average power is positive. The non-zero SC average power results in an energy difference of about 0.01 kWh between the start and the end of this simulation.

The experimental results of the FC/SC passive configuration under a downscaled Artemis Urban drive cycle current are shown in Fig. 13. As shown in Fig. 13 (a), when the load current changes frequently, the SC bank reacts to this high-frequency change while the current and power of the FC change gradually due to its relatively higher internal resistance. The maximum FC current/power change rate is 1.6 A/s and 82.4 W/s, which is only 2.3% and 2.7% of the nominal current/power per second, respectively. Therefore, the FC degradation is reduced in this passive hybrid configuration. The current distributions between simulation and experiment with the same initial conditions are compared in Fig. 13 (b) and the simulation shows good consistent with the experiment. The histograms in Fig. 13 (c) shows that the FC supplies almost the average power of the load while the SC provides nearly zero average power. This results in an energy difference of 0.005 kWh during this drive cycle test. Since the SC handles most of the peak power, the FC can be downsized. In fact, the FC peak power is only about one third of the load peak power.

5. Conclusions

This paper deals with the design and characterization of a passive FC/SC configuration for a 60 V light vehicle. The detailed test procedure is developed. The FC and SC models are experimentally characterized and verified. Simulations results using these models match the experimental data well. The dynamic response of the FC stack is characterized as a combination of the resistive characteristics and a first-order system. The behavior of the SC bank is simulated by resistors and capacitors connected in series. It turns out that the internal resistance of the SC bank is around 10 times smaller than that of the FC stack.

The feasibility of the FC/SC passive configuration is experimentally verified when a step load current is applied: the SC bank provides the transient current and power while the FC stack takes over the steady-state current and power. The FC/SC passive configuration allows the FC to have a long stabilization time and to avoid the OCV operation, which can reduce the FC degradation and improve the FC lifetime. The FC/SC passive configuration is further simulated and experimentally verified under the Artemis Urban drive cycle. Results show that the low-pass filter effect makes it possible to downsize the FC stack, which only needs a peak power of one third of the load peak power. The SC evens

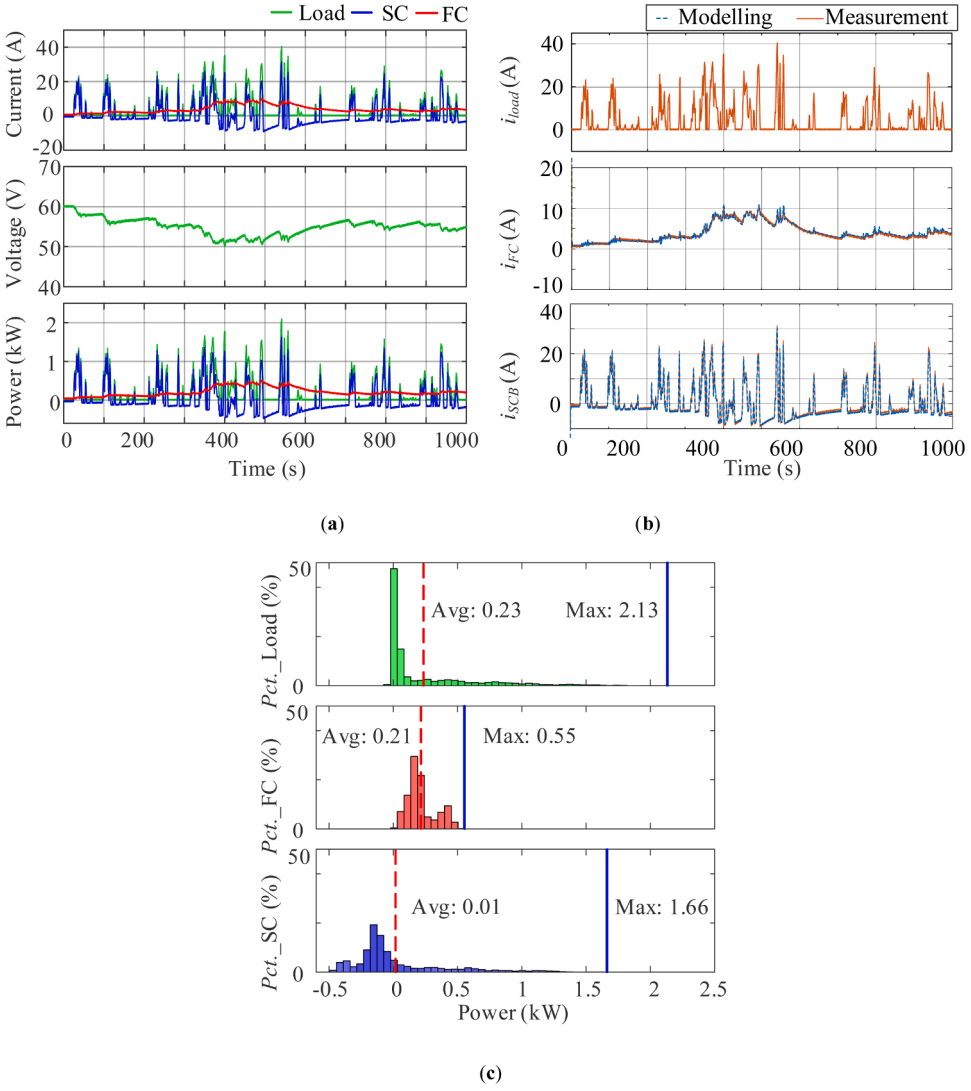

Fig. 13. Experimental results of the passive hybrid system under Artemis Urban drive cycle: (a) Current, voltage and power distribution; (b) Current distributions; (c) Histograms of power.

out the current and power from the FC to prevent the FC from experiencing large currents and power variations.

Future work related to this paper will be focused on several aspects. First, a four-quadrant electronic load needs to be introduced to validate the performance of the FC/SC passive system under various drive cycles with regenerative braking. Second, properly size of the FC stack and the SC bank should be designed to optimize the cut-off frequency. Third, to achieve a better controllability, active hybrid topologies may be required while passive hybrid configurations would be better for applications where the travel route and operation speed are pre-defined.

6. Outlook and future trends

In the past few decades, FCEVs have made significant progress in terms of environmental adaptability, driving range, and performance. FCEVs have achieved - 40°C cold start. Heat dissipation at high temperatures is no longer an issue. The driving range has been extended due to the development of the hydrogen tank. In today's passenger car, the hydrogen tank volume has increased to 60 L, the pressure has increased to 700 bar, and the mass ratio of hydrogen and tank has increased to 5.7%. With improvements in the power density of FC, power converter, and electric machine, the size and weight of FCEVs are also reduced. However, there are still some challenges for the development of FCEVs. The durability of FCEVs has not met the DoE target due to the relatively short lifetime of the FC stack. Hydrogen refueling infrastructure needs to be expanded. In fact, only 432 stations have been established by the end of 2019 although more stations are expected to be established in the future. One of the biggest concerns is the relatively high cost of FCEVs (e.g., 6000 USD for a Mirai). Therefore, lifetime enhancement of the FC stack, establishment of hydrogen stations and cost reduction of FCEVs are some of the main challenges.

As reported in this paper, great efforts have been made to optimize different hybridization topologies between FC, battery, and SC as well as power control and energy management strategies. On the other hand, further improvements in the performance of these power devices are still required. In fact, li-ion battery/SC hybrid device is being developed to fully take advantage of battery and SC. With the hybridization of FC and Li-ion SC, the power density and energy density of the FCEV powertrain can be improved, which will significantly enhance the driving range and the dynamic response.

Funding

This work was supported by the Swedish Electromobility Center and the Swedish Energy Agency.

Author statement

Q.X. and Y.L. conducted the investigation and the conceptualization, Q.X. and S.L participated in the experiment and validation. Q.X. wrote the original draft and S.L. and Y.L. participated in the review & editing.

Declaration of Competing Interest

The authors declare that they have no known competing financial interests or personal relationships that could have appeared to influence the work reported in this paper.

Acknowledgements

The authors would like to thank the master's students Denis Hafizovic, Georgios Mamolis, Kunyang Huang and Yuning Li for participating in data collection.

References

[1] B.K. Ahn, T.W. Lim, Fuel cell vehicle development at Hyundai-Kia motors, Int. Forum Strat. Technol. Ulsan (2006) 199–201, https://doi.org/10.1109/IFOST.2006.312284.
[2] Q. Xun, Y. Liu, E. Holmberg, A comparative study of fuel cell electric vehicles hybridization with battery or supercapacitor, in: Proceedings of International Symposium on Power Electronics, Electrical Drives, Automation and Motion (SPEEDAM), 2018, pp. 389–394.
[3] J.M. Kurtz, S. Sprik, G. Saur, et al., Fuel cell electric vehicle durability and fuel cell performance, Natl. Renew. Energy Lab (NREL) Technical Rep. (Mar. 2019).
[4] W.G. Colella, M.Z. Jacobson, D.M. Golden, Switching to a U.S. hydrogen fuel cell vehicle fleet: the resultant change in emissions, energy use, and greenhouse gases, J. Power Sources 150 (2005) 150–181.
[5] Q. Li, W. Yang, W. Chen, Real-time implementation of maximum net power strategy based on sliding mode variable structure control for proton-exchange membrane fuel cell system, IEEE Trans. Transp. Electr. 6 (1) (2020) 288–297.
[6] H.S. Das, C.W. Tan, A.H.M. Yatim, Fuel cell hybrid electric vehicles: a review on power conditioning units and topologies, Renewable Sustainable Energy Rev. 76 (2017) 268–291.
[7] H. Takenaka, Research on electric power system for Honda FCX fuel cell vehicle, Honda R&D Tech. Rev. vol.15 (2) (2003) 1–6.
[8] A. Ohkawa, Electric power control system for a fuel cell vehicle employing electric double-layer capacitor, SAE World Congress (2004). SAE 2004-01-1006.
[9] https://global.honda/innovation/FuelCell/Clarity-Fuel-Cell-engineer-talk.html.
[10] Hiroyuki Yumiya, Mikio Kizaki, Hisao Asai, Toyota fuel cell system (TFCS), World Electr. Veh. J. vol.7 (2015) 1–8.
[11] Y. Nonobe, Development of the fuel cell vehicle Mirai, IEEJ Trans. Electr. Electron. Eng. 12 (2017) 5–9.
[12] NEXO Emergency response guide, available online: https://h2tools.org/sites/default/files/NEXO%20Emergency%20Response%20Guide.pdf.
[13] M. Ouyang, L. Xu, J. Li, et al., Performance comparison of two fuel cell hybrid buses with different powertrain and energy management strategies, J. Power Sources 163 (1) (2006) 467–479.
[14] D.F. Pereira, F.C. Lopes, E.H. Vantanabe, Nonlinear model predictive control for the energy management of fuel cell hybrid electric vehicles in real-time, IEEE Trans. Ind. Electron. (Mar. 2020), https://doi.org/10.1109/TIE.2020.2979528. Early Access.
[15] H. Chen, J. Chen, H. Lu, et al., A modified MPC-based optimal strategy of power management for fuel cell hybrid vehicles, IEEE/ASME Trans. Mechatron. 25 (4) (2020), 2009–2018.
[16] X. Wu, X. Hu, X. Yin, et al., Convex programming improved online power management in a range extended fuel cell electric truck, J. Power Sources 476 (2020), 228642.
[17] T. Azib, O. Bethous, G. Remy, et al., An innovative control strategy of a single converter for hybrid fuel cell/supercapacitor power source, IEEE Trans. Ind. Electron. 57 (12) (2010) 4024–4031.
[18] M. Marx, M. Özbek, D. Söffker, Power management of a hybrid electric powertrain system-design, power flow control, and optimization targets, Int. J. Powertrains 3 (2) (2014) 221–241.
[19] X. Hu, C. Zou, X. Tang, et al., Cost-optimal energy management of hybrid electric vehicles using fuel cell/battery health-aware predictive control, IEEE Trans. Power Electron. 35 (1) (2020) 382–392.
[20] Q. Li, B. Su, Y. Pu, et al., A state machine control based on equivalent consumption minimization for fuel cell/supercapacitor hybrid tramway, IEEE Trans. Transp. Electrification 5 (2) (2019) 552–564.
[21] Y. Yan, Q. Li, W. Chen, et al., Optimal energy management and control in multimode equivalent energy consumption of fuel cell/supercapacitor of hybrid electric tram, IEEE Trans. Ind. Electron. 66 (8) (2019) 6065–6076.
[22] Q. Li, W. Chen, Y. Li, et al., Energy management strategy for fuel cell/battery/ultracapacitor hybrid vehicle based on fuzzy logic, Electr. Power Energy Syst. 43 (2012) 514–525.
[23] X. Hu, L. Johannesson, N. Murgovski, et al., Longevity-conscious dimensioning and power management of the hybrid energy storage system in a fuel cell hybrid electric bus, Appl. Energy 137 (2015) 913–924.
[24] Q. Li, H. Yang, Y. Han, et al., A state machine strategy based on droop control for an energy management system of PEMFC-battery-supercapacitor hybrid tramway, Int. J. Hydrogen Energy (2016) 1–12.
[25] Q. Li, T. Wang, C. Dai, et al., Power management strategy based on adaptive droop control for a fuel cell-battery-supercapacitor hybrid tramway, IEEE Trans. Veh. Technol. 67 (7) (2018) 5658–5670.
[26] F. Zhang, X. Hu, R. Langari, et al., Energy management strategies of connected HEVs and PHEVs: recent progress and outlook, Prog. Energy Combust. Sci. 73 (2019) 235–256.
[27] H. Zhao, A.F. Burke, Fuel cell powered vehicle using supercapacitors-device characteristics, control strategies, and simulation results, Fuel Cells 10 (5) (2010) 879–896.
[28] Q. Xun, Y. Liu, N. Zhao, Energy efficiency comparison of hybrid powertrain systems for fuel-cell-based electric vehicles, in: IEEE Transportation Electrification Conference & Expo (ITEC), Jun., 2020, pp. 23–26.
[29] A. Macías, M. Kandidayeni, L. Boulon, et al., Passive and active coupling comparison of fuel cell and supercapacitor for a three-wheel electric vehicle, Fuel Cells 20 (3) (2020) 351–361.
[30] E.L. Gonzalez, J.S. Cuesta, F.J.V. Fernandez, et al., Experimental evaluation of a passive fuel cell/battery hybrid power system for an unmanned ground vehicle, Int. J. Hydrogen Energy 44 (25) (2018) 1–11.

[31] J. Bernard, M. Hofer, U. Hannesen, et al., Fuel cell/battery passive hybrid power source for electric powertrains, J. Power Sources 196 (2011) 5867–5872.
[32] A. Nishizawa, J. Kallo, O. Garrot, et al., Fuel cell and li-ion battery hybridization system for aircraft applications, J. Power Sources (222) (2013) 294–300.
[33] R.C. Samsun, C. Krupp, S. Baltzer, et al., A battery-fuel cell hybrid auxiliary power unit for trucks: analysis of direct and indirect hybrid configurations, Energy Convers. Manage. 127 (2016) 312–323.
[34] Y. Chen, S. Lin, B. Hong, Experimental study on a passive fuel cell/battery hybrid power system, Energies 6 (2013) 6413–6422.
[35] W. Zuo, R. Li, C. Zhou, et al., Battery-supercapacitor hybrid devices: recent progress and future prospects, Adv. Sci. 4 (7) (2017) 1–21.
[36] D. Arora, C. Bonnet, M. Mukherjee, et al., Direct hybridization of PEMFC and supercapacitors: effect of excess hydrogen on a single cell fuel cell durability and its feasibility on fuel cell stack, Electrochim. Acta 310 (2019) 213–220.
[37] K. Gérardin, S. Raël, C. Bonnet, Direct coupling of PEM fuel cell to supercapacitors for higher durability and better energy management, Fuel Cells 18 (3) (2018) 315–325.
[38] B. Morin, D. Van Laethem, C. Turpin, et al., Direct hybridization fuel cell-ultracapacitors, Fuel Cells 14 (3) (2014) 500–507.
[39] C. Turpin, D. Van Laethem, B. Morin, et al., Modeling and analysis of an original direct hybridization of fuel cells and ultracapacitors, Math. Comput. Simul 131 (2017) 76–87.
[40] D. Arora, M. Hinaje, C. Bonnet, et al., Sizing supercapacitor for direct hybridization with polymer electrolyte membrane fuel cell, in: IEEE Vehicle Power and Propulsion Conference (VPPC), 2018, pp. 1–7.
[41] M.G. Arregui, C. Turpin, S. Astier, Direct connection between a fuel cell and ultracapacitors, in: International Conference on Clean Electrical Power, 2007, pp. 474–479.
[42] B. Wu, M.A. Parkes, V. Yufit, et al., Design and testing of a 9.5 kWe proton exchange membrane fuel cell-supercapacitor passive hybrid system, Int. J. Hydrogen Energy 39 (2014) 7885–7896.
[43] C. Dépature, A Macías, A Jácome, et al., Fuel cell/supercapacitor passive configuration sizing approach for vehicular applications, Int. J. Hydrogen Energy 45 (2020) 1–12.
[44] Q. Xun, Y. Liu, Evaluation of fluctuating voltage topology with fuel cells and supercapacitors for automotive applications, Int. J. Energy Res. 43 (2019) 4807–4819.
[45] Q. Xun, Y. Liu, X. Huang, et al., Drive cycle energy efficiency of fuel cell/supercapacitor passive hybrid vehicle system, IEEE Trans. Ind. Appl. (2020), https://doi.org/10.1109/TIA.2020.3035551. Early Access.
[46] https://www.car.info/en-se/renault/twizy/twizy-urban-80-6614518/specs.
[47] https://evcompare.io/cars/renault/renault_twizy_URBAN/.
[48] E.A. Grunditz, T. Thiringer, Characterizing BEV powertrain energy consumption, efficiency, and range during official and drive cycles from Gothenburg, Sweden, IEEE Trans. Veh. Technol. 65 (6) (2016) 3964–3980.
[49] J.Y. Wong (Ed.), Theory of Ground Vehicles, 4th ed, John Wiley & Sons, Inc., 2008.
[50] T.D. Gillespie, Fundamentals of Vehicle Dynamics, 1st ed, Society of Automotive Engineers, Inc., 1992.
[51] Horizon Technology, 3000 W fuel cell stack user manual. Online available: https://www.fuelcellstore.com/manuals/horizon-pem-fuel-cell-h-3000-manual.pdf.
[52] Maxwell Technologies Ultracapacitors. BCAP3000 datasheet. 3000F, 2.7V. Available online:https://www.maxwell.com/images/documents/K2Series_DS_1015370_5_20141104.pdf. Accessed 2014-11-04.
[53] https://www.mathworks.com/help/physmod/sps/powersys/ref/fuelcellstack.html.
[54] F. Khan, A. Nawaz, M.A. Muhammad, et al., Review and analysis of MATLAB® Simulink model of PEM fuel cell stack, Int. J. Eng. Comput. Sci. IJECS-IJENS 13 (3) (2013) 31–34.
[55] A. Kirubakaran, S. Jain, R.K. Nema, The PEM fuel cell system with DC/DC boost converter: design, modelling and simulation, Int. J. Electr. Power Eng. 1 (1) (2010) 26–30.
[56] O Leena, P.Koujalagi Jyoti, Modelling and simulation of hydrogen fuel cells, Int. J. Eng. Sci. Invention 3 (6) (2014) 14–23.
[57] Q. Li, T. Wang, C. Dai, et al., Power management strategy based on adaptive droop control for a fuel cell-battery-supercapacitor hybrid tramway, IEEE Trans. Veh. Technol. 67 (7) (2018) 5658–5670.
[58] S.N. Motapon, L.A. Dessaint, K. Al-Haddad, A comparative study of energy management schemes for a fuel-cell hybrid emergency power system of more-electric aircraft, IEEE Trans. Ind. Electron. 61 (3) (2014) 1320–1334.
[59] https://www.mathworks.com/help/physmod/sps/powersys/ref/supercapacitor.html.
[60] V. Sedlakova, J. Sikula, J. Majzner, et al., Supercapacitor degradation assessment by power cycling and calendar life tests, Metrol. Meas. Syst. 23 (3) (2016) 345–358.
[61] X. Zhang, D. Yang, M. Luo, et al., Load profile based empirical model for the lifetime prediction of an automotive PEM fuel cell, Internal J. Hydrogen Energy 42 (2017) 11868–11878.